Shedding Light on Membrane-Templated Clustering of Gold Nanoparticles

Costanza Montis[a+], *Lucrezia Caselli*[a+], *Francesco Valle*[b], *Andrea Zendrini*[c], *Francesco Carlà*[d], *Ralf Schweins*[e], *Marco Maccarini*[f], *Paolo Bergese*[c] *, *Debora Berti*[a] *

[a] Department of Chemistry and CSGI, University of Florence via della Lastruccia3, 50019 Florence (Italy); [b] ISMN-CNR and CSGI via Gobetti 101 40129 Bologna (Italy); [c] Department of Molecular and Translational Medicine, University of Brescia, Viale Europa 11, 25123 Brescia, Italy; [d] ESRF, The European Synchrotron, Grenoble (France); [e] Institut Laue-Langevin, DS/LSS, 71 Avenue des Martyrs, CS 20156, F-38042 Grenoble CEDEX 9, (France); [f] Univ. Grenoble Alpes, CNRS, TIMC-IMAG-SyNaBi (UMR 5525), 38000 Grenoble, France

Corresponding Authors *** debora.berti@unifi.it; paolo.bergese@unibs.it**

CRediT author statement

Costanza Montis: Conceptualization, design of experiments, optical spectroscopy, QCM (PSCMlab), SANS (ILL), XRR (ESRF), SAXS and AFM investigations, analysis and interpretation of data; Original draft preparation, Writing original draft. **Lucrezia Caselli:** design of experiments; optical spectroscopy, SAXS, QCM (PSCMlab) and AFM investigation; analysis and interpretation of data; Original draft preparation. **Francesco Valle**: AFM and XRR (ESRF) investigation, data analysis and interpretation. **Andrea Zendrini**: SANS Investigation (ILL). **Francesco Carlà**: XRR investigation (ESRF), XRR data analysis and interpretation**. Ralf Schweins**: SANS investigation (ILL), SANS data analysis and interpretation. **Marco Maccarini**: SANS investigation (ILL), SANS data analysis and interpretation. **Paolo Bergese**: Conceptualization, Funding acquisition, Methodology, Supervision, Writing original draft. **Debora Berti**: Conceptualization, Funding acquisition, Methodology, Design of Experiments, Analysis and interpretation of data, Supervision, Writing original draft

All authors have given approval to the final version of the manuscript. CM and LC contributed equally to this work.

ABSTRACT The use of inorganic nanoparticles in biomedical and biotechnological applications requires a molecular-level understanding of interactions at nano-bio interfaces, such as cell membranes. Several recent reports have shown that gold nanoparticles (AuNPs), in the presence of fluid lipid bilayers, aggregate at the lipid/aqueous interface, but the precise origin of this phenomenon is still not fully understood. Here, by challenging synthetic lipid membranes with one of the most typical classes of nanomaterials, citrate-coated AuNPs, we addressed the cooperative nature of their interaction at the interface, which leads to AuNPs' clustering. The ensemble of optical (UV-Vis absorbance), structural (small-angle neutron and X-ray scattering) and surface (X-ray reflectivity, quartz crystal microbalance, atomic force microscopy) results, is consistent with a mechanistic hypothesis, where the citrate-lipid ligand exchange at the interface is the molecular origin of a multiscale cooperative behavior, which ultimately leads to the formation of clusters of AuNP on the bilayer. This mechanism, fully consistent with the data reported so far in the literature for synthetic bilayers, would shed new light on the interaction of engineered nanomaterials with biological membranes. The cooperative nature of ligand exchange at the AuNP-liposome interface, pivotal in determining clustering of AuNP, will have relevant implications for NP use in Nanomedicine, since NPs will be internalized in cells as clusters, rather than as primary NP, with dramatic effects on their bioactivity.

KEYWORDS: Gold Nanoparticles; Lipid Bilayers; Surface Plasmon Resonance; Membranes; Nano-Bio interface

1. INTRODUCTION

Understanding the behavior of nanomaterials in biological environments is a longstanding research challenge, necessary to fully harness the medical potential of nanomaterials and rationally assess their cytotoxicity [1–3]. In particular, interactions at the nano-bio interface are recognized as pivotal steps to determine the fate of nanostructured materials in living systems[4–7]. In this respect, the study of interactions of nanomaterials with synthetic lipid membranes can contribute robust fundamental knowledge and help identifying some of the main factors implied in the behavior in biological systems [6–9].

Turkevich-Frens gold nanoparticles coated with a layer of citrate anions, (AuNP), are one of the most studied and explored class of inorganic nanoparticles for biomedical applications. Upon incubation with lipid membranes, they can exhibit an intriguing behavior: the presence of lipid vesicles affects the optical properties of the AuNP, displayed as a shift of the surface plasmon resonance, with a marked color variation of the dispersion[10–14]. This effect, a clear signature of membrane-templated clustering of AuNP [13,15], is relevant both from a fundamental and from an applicative perspective. The clustering of NP is a relevant feature that determines their cell internalization pathway [4,16]; moreover, some technological applications of this membrane-induced aggregation are already in use, like in a recently developed analytical assay to estimate the purity and concentration of extracellular vesicles[17].

Despite the number of studies on citrated AuNP and the fundamental and applicative implications of their clustering, occurring in the presence of natural and synthetic lipid membranes, this phenomenon has started to be addressed only recently [12,13,18]. These investigations have provided evidence that AuNP aggregation on lipid membranes eventually leads to the formation of an AuNP

crust on the target membrane [13] and that the clustering extent depends on membrane fluidity [10,14] and nature of the coating agent [12]. However, a thorough mechanistic understanding of the phenomenon, which reconciles the experimental observations reported so far, is still lacking.

In this study we present a comprehensive investigation of the interaction of AuNP with synthetic free-standing and supported bilayers composed of POPC (1-palmitoyl-2-oleoyl-glycero-3-phosphocholine), which results in AuNP clustering. Combining optical (UV-Vis absorbance), structural (small-angle neutron and X-ray scattering) and surface (X-ray reflectivity, quartz crystal microbalance, atomic force microscopy) techniques, we disentangle the main probabilistic, kinetic and thermodynamic contributions. In addition, based on the ensemble experimental results here presented, we propose an original hypothesis on the molecular mechanism of the bilayer-driven clustering, whose key step is identified as the POPC-citrate ligand exchange.

2. MATERIALS AND METHODS

2.1 Materials

Tetrachloroauric (III) acid (≥ 99.9%), trisodium citrate dihydrate (≥ 99.9%), MeOH (99.8%), $CHCl_3$ (≥ 99.9%), NaCl (≥99.5%), $CaCl_2$ (99.999%) and D_2O (99 atom % D) were provided by Sigma-Aldrich (St. Louis, MO). The same for 1-palmitoyl-2-oleoyl-sn-glycero-3-phosphocholine (POPC) (≥ 98.0%), tannic acid (99.8%) and 3-mercaptopropionic acid (MPA) (99.0%). All chemicals were used as received. Milli-Q grade water was used in all preparations.

2.2 Synthesis of AuNP

Citrated gold nanospheres of 16 nm diameter were synthesized according to the classical Turkevich-Frens protocol [19,20], whose details are reported in the SI (page S2 of Supplementary

Materials and Methods section). To obtain 16 nm MPA-capped AuNP the following method was adopted: 500 µL of an aqueous solution of 3-mercaptopropionic acid ($5x10^{-3}$ M) were added to 5 ml of freshly prepared 16 nm-citrated AuNP ($7.8 \cdot 10^{-9}$ M). The mixture was stirred for 30 s and left at 4°C overnight. To obtain smaller citrated NP (5 nm diameter), a slightly different procedure was adopted, with addition of tannic acid traces to the inverse Turkevich method [21]. Briefly, 1 mL of $HAuCl_4$ aqueous solution (25 mM) was injected into 150 mL of sodium citrate aqueous solution (2.2 mM), mixed with 0.1 mL of tannic acid (2.5 mM). The addition was carried out at 70°C under vigorous magnetic stirring and led to the instantaneous color change of the solution from transparent to dark grey. After a few minutes, the solution turned orange, indicative of the formation of sub-10 nm gold nanoparticles. The nanoparticles solution was then slowly cooled down to room temperature.

2.3 Preparation of POPC vesicles and Supported Lipid Bilayers (SLB)

For POPC liposomes preparation, a standard method of dry film rehydration was adopted, followed by freeze-thaw cycles and extrusion (see page S3 of SI for details). For SLBs formation a similar procedure was adopted: briefly, a dry lipid film of POPC was suspended in warm (50°C) aqueous solution containing 100 mM NaCl by vigorous vortex mixing and then tip-sonicated for 30 minutes. SLBs were prepared by adding 10 mM $CaCl_2$ to the vesicles' dispersion and subsequently depositing a droplet of the vesicles' dispersion on a silicon wafer previously polished and activated in a plasma cleaner. A stable SLB layered on the support was obtained by rinsing the vesicles' dispersion with pure milliQ water, after incubation of the vesicles with the support for twenty minutes at room temperature. Further details are reported in the SI (page S3).

2.4 Small Angle X-ray Scattering

SAXS measurements were carried out on a S3-MICRO SAXS/WAXS instrument (HECUS GmbH, Graz, Austria) which consists of a GeniX microfocus X-ray sealed Cu Kα source (Xenocs, Grenoble, France) of 50 W power which provides a detector focused X-ray beam with $\lambda = 0.1542$ nm Cu Kα line. The instrument is equipped with two one-dimensional (1D) position sensitive detectors (HECUS 1D-PSD-50 M system), each detector is 50 mm long (spatial resolution 54 μm/channel, 1024 channels) and cover the SAXS q-range ($0.003 < q < 0.6$ ˚Å $^{-1}$). The temperature was controlled by means of a Peltier TCCS-3 Hecus. The analysis of SAXS curves was carried out using Igor Pro [22]. Details on the measurements and data analysis are reported in the SI (see page S10 of Supplementary Characterization of Gold Nanoparticles).

2.5 Small Angle Neutron Scattering

SANS experiments were performed on D11 at the Institut Laue – Langevin (Grenoble, France). All measurements have been done at 25°C in cylindrical quartz cuvettes of 1mm path length. A neutron beam size of 13mm in diameter has been employed. Three instrument settings were used, all with a neutron wavelength of 6 Å, having a FWHM of 9%. The sample to detector distances were 1.5 m, 8 m and 39 m with corresponding collimation distances of 5.5 m, 8 m and 40.5 m respectively. Scattered intensities were collected with a MWPC ^{3}He detector with $128 \cdot 128$ pixels of $7.5 \cdot 7.5$ mm^2 size. Data were normalized with respect to the measurement of a 1mm path length MilliQ H_2O cuvette, for which the differential scattering cross section for 6 Å on D11 has been determined to 0.983 cm^{-1} via a cross calibration against h/d polymer blends. Data reduction was done using the LAMP software package available at the Institut Laue – Langevin. All data were corrected for the scattering of a dark current, as a background the scattering of an empty cell has been subtracted. In a second step the data were radially averaged and the scattering from the

background (D_2O) has been subtracted. Transmissions were measured at a sample to detector distance of 8 m with a collimation distance of 8 m.

2.6 X-ray Reflectivity

XRR experiments were performed at the ID03 surface diffraction beamline of the ESRF. The experiments were conducted using the six-circle diffractometer with vertical scattering geometry of experimental hutch 1. During the experiment a drop of buffer solution was maintained on the sample surface. In order to minimize the beam damage a 24keV x-ray beam de-focused in the horizontal plane has been used, with a resulting beam size of 45x600 μm^2 at the sample position. These conditions have been already successfully used to characterize similar samples in analogue conditions [23,24]. The images were collected using a Maxipix camera (ESRF) (2x2 chips, 516x516 pixels) at a distance of 772 mm from the sample. The software MOTOFIT was employed for the analysis of the XRR curves. Details on data analysis are reported in the SI (page S19 of Supplementary Data Analysis).

2.7 Atomic Force Microscopy liquid imaging

AFM experiments in liquid were performed at the SPM@ISMN facility in Bologna using a Multimode VIII (Bruker, Santa Barbara, CA, US) and at the Partnership for Soft Condensed Matter (PSCM) in Grenoble using a Cypher S (Asylum Research, Santa Barbara, CA, US). In the first case images were collected in peakforce tapping using SNL Bruker cantilevers with nominal spring constant of 0.24 N/m and 2-10 nm curvature radius, in the second one Olympus BL-AC40TS cantilevers were chosen to perform tapping mode imaging. Details on samples preparation and image analysis are reported in the SI (page S8 of Supplementary Materials and Methods).

2.8 Quartz Crystal Microbalance with Dissipation Monitoring (QCM-D)

QCM-D experiments were performed on a Q-Sense E4 instrument (Q-Sense, Gothenburg, Sweden) in the Partnership for Soft Condensed Matter Laboratory (PSCM) Grenoble (France) [25–27]. The instrument was equipped with four flow liquid cells (0.5ml internal volume), each containing a coated quartz sensor with 4.95 MHz fundamental resonance frequency, mounted horizontally. The active surface of the sensors (~1 cm^2) was coated with a thin SiO_2 layer (~100 nm thick). The sensors were cleaned prior to use by ozone cleaning, bath sonication in chloroform, acetone and ethanol and extensively rinsed with MilliQ water and ethanol. The experiments were performed at 18°C and solvent exchange in the measurement chamber was achieved with a peristaltic pump. First, the sensors were placed in the chambers and water was injected at a low flow rate (0.07 ml/min), the frequencies (f) and corresponding energy dissipation factors (D) were measured for the odd harmonics (1st–13th). A stable baseline for both f and D of the different harmonics was ensured before injection of the vesicles. The QCM-D curves reported are normalized by the overtone number. Details on data analysis are reported in the SI (page S9 of Supplementary Materials and Methods).

3. RESULTS AND DISCUSSION

3.1. UV-Vis characterization of liposomes-induced clustering of AuNP

After mixing a 1.3 nM dispersion of negatively charged citrated AuNP (16 nm diameter, zeta potential: -36 ± 2 mV,) with 100 nm-sized zwitterionic POPC liposomes (zeta potential: -4.9 ± 0.4), we monitored the spectral variations in the region of the plasmon resonance band of AuNP. Figure 1 shows the observed changes, as several factors and/or experimental conditions were

varied, in particular: (i) POPC liposomes/AuNP ratio (*R*) (Figure 1a, 1b), (ii) mixing sequence (Figure 1c), (iii) volume of the solution (Figure 1d, 1e) (see pages S3-S6 of SI for details of the preparation of samples).

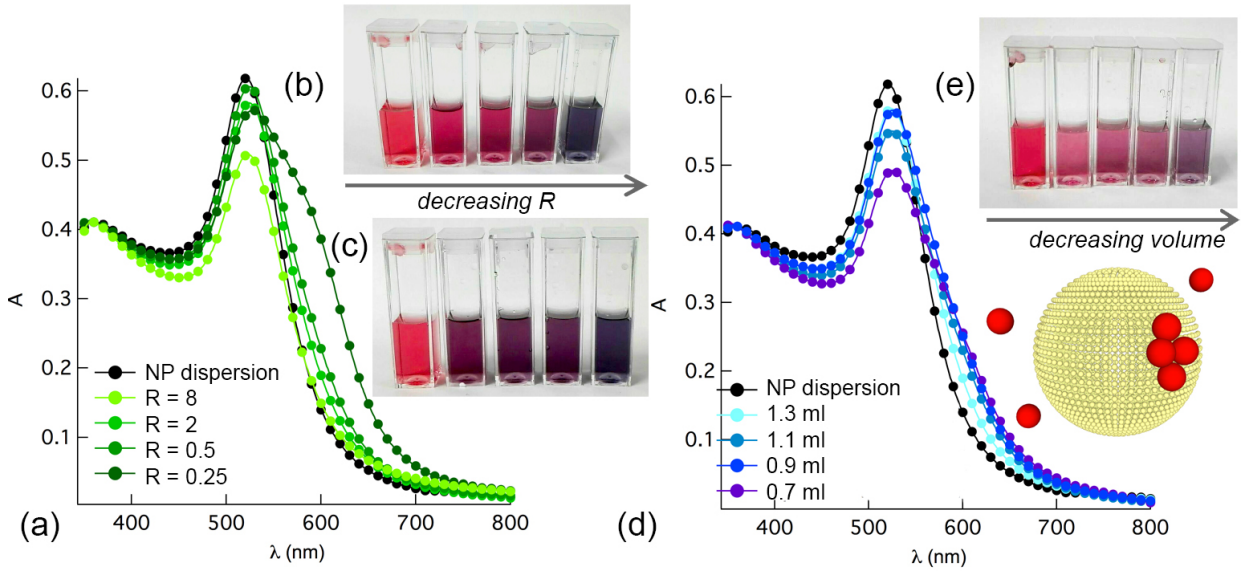

Figure 1. UV-Vis characterization of AuNP-POPC vesicles interaction. UV-Vis spectra of AuNP (1.3 nM) in the presence of different amounts of POPC liposomes (*R* = 8; 2; 0.5, and 0.25) and visual appearance of the corresponding samples (b, c). (d) UV-Vis spectra of Lipo/AuNP *R* = 2 complexes, initially mixed in different volumes, and then diluted to the same final volume and visual appearance of the corresponding samples (e).

The reference sample is a 1.3 nM dispersion of AuNP in water, where the negative charge of citrate coating provides electrostatic stabilization (black curves, Figure 1a, 1d) which prevents NP aggregation. In this sample, the absorbance is characterized by an intense and defined surface plasmon band at 521 nm, typical of colloidally stable gold particles of nanometric size. The addition of decreasing amounts of liposomes causes a progressive broadening of the plasmon

resonance peak and, eventually, the appearance of a redshifted shoulder (Figure 1a). The observed shift, due to plasmon-plasmon coupling, originates from the spatial proximity of NP and is the hallmark of NP aggregation. This effect has been already observed in several reports [10–12,14] showing that, for defined experimental conditions, AuNP will cluster on the liposomal surface. Here, in line with a recent study [12], we show that the extent of clustering, also detectable by the naked eye as a red-to-blue color change of the dispersion (Figure 1b), strictly depends on the relative amounts of liposomes and AuNP (Figure 1a). In contrast to salt-induced aggregation of AuNP, which is maximized increasing the ionic strength, this shift is maximum for the lowest amounts of added liposomes. This is a clear indication that the clustering of AuNP is a membrane-dependent phenomenon, which strictly occurs on the liposomal surface, so that the lower the liposomal surface extension available, the higher the aggregation extent of AuNP.

Up to now, reports on membrane-induced clustering of citrated AuNP have focused mainly on energetics. For instance, it has been shown that the interaction is inhibited if the lipid membrane is negatively charged, accounting for an electrostatic repulsive contribution [10,15]; that the clustering depends on the phase properties of the target, i.e., the melting temperature of the composing lipid bilayer [14,18]; that the chemical nature of the coating agent affects the affinity of AuNP with the target membrane [11,15]; that the adhesion of NP might affect the phase behavior of the target membrane [13,28,29].

With respect to these previous contributions, the experimental results shown here provide additional details: in particular, kinetic effects are of prominent relevance. In fact, the mixing order of the species (i.e., liposomes added to the AuNP solution (Figure 1c) vs AuNP added to the liposome solution (Figure 1b)) determines meaningful differences in the extent of NP clustering, which do not disappear even after one week incubation (data not shown), suggesting that the

membrane-induced aggregation of AuNP is irreversible and does not evolve to a more thermodynamically stable state, in the time frame of our experimental observations. To strengthen this conclusion, we observed that a variation of the volume at which AuNP and liposomes are initially mixed (see page S3 of SI for the detailed preparation of samples) strongly affects the extent of NP clustering in a similarly irreversible fashion. Specifically, liposomes/AuNP hybrids of Figure 1d-e were incubated at different volumes, modifying liposomes and AuNP concentrations during mixing, but not their relative numerical ratio, and then diluted to the same final volume: the reduction of the interaction volume is associated to larger variations of the spectral properties which are not leveled after one week, providing further evidence of the irreversible nature of the AuNP aggregation process.

While it is clear from the recent literature that thermodynamic contributions, as NP-membrane and NP-NP Van der Waals attractive forces, are involved in AuNP docking to the membrane and AuNP-AuNP aggregation on the liposomal surfaces, both the kinetic control and the irreversible nature of the process have been so far unaddressed, to the best of our knowledge.

3.2. Structural characterization of AuNP-liposome aggregates

SAXS, SANS and AFM were used to investigate the structure of AuNP-POPC liposome dispersions. (Figure 2). In recent studies, Cryo-EM was also used to visualize AuNP clusters on liposomes [12,14,18]. Here we provide an ensemble-averaged description, combining solution ensemble techniques (SAXS and SANS) with atomic force microscopy (liquid AFM). SAXS and SANS provide complementary structural information at the nanoscale: the high AuNP/H_2O contrast in SAXS emphasizes the structural features of the NP and of their aggregates, if present,

whereas the high lipid/D_2O contrast in SANS provides access to structural details of the NP effects on the lipid bilayers.

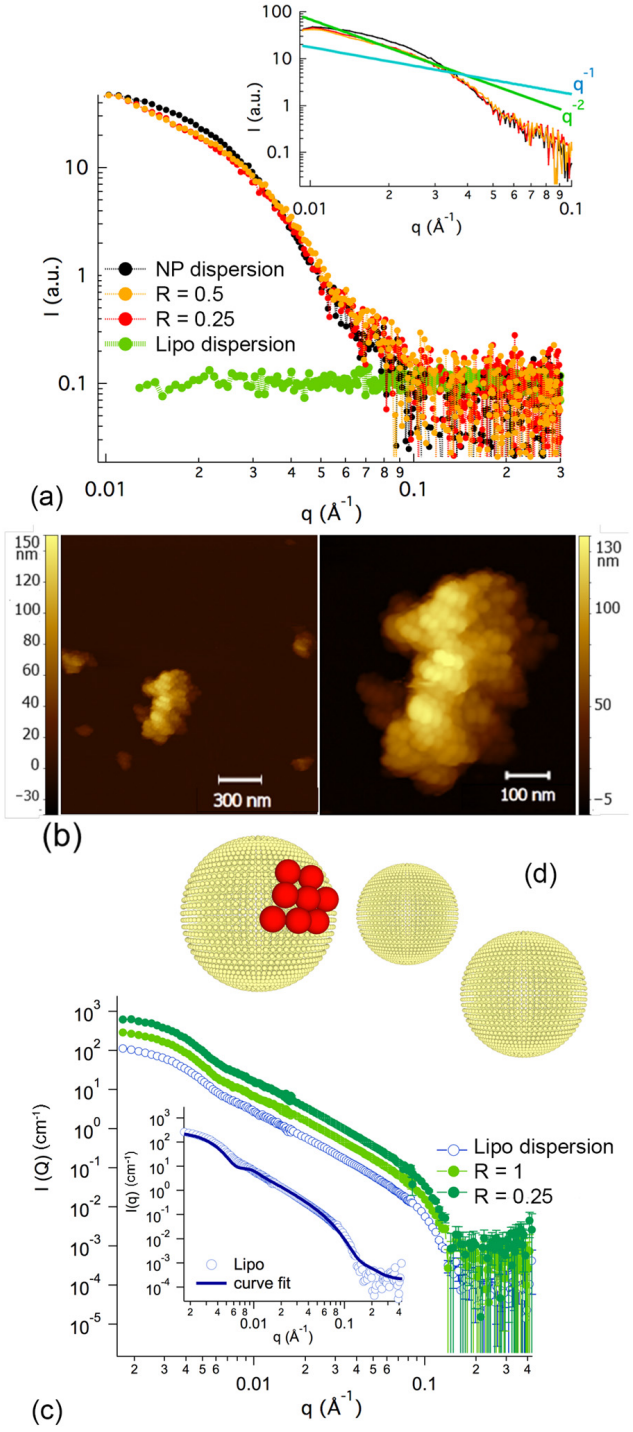

Figure 2. Structural characterization of AuNP-POPC liposome complexes. (a) SAXS of POPC liposomes in the presence of different amounts of AuNP (R = 0.5 and 0.25); comparison of the experimental curves with the power laws $I(q) \propto q^{-1}$ and $I(q) \propto q^{-2}$ (inset). (b) Representative AFM images of POPC liposomes after interaction with AuNP (R = 0.25); magnification of the AFM image which highlight the AuNP aggregates. (c) SANS profiles of POPC liposomes in the presence of different amounts of AuNP (R = 1 and 0.25); the curve fit for liposomes according to a polydisperse core-shell model is consistent with vesicles of a 45 nm radius and polydispersity 0.3 according to a Schulz distribution (inset)". SANS measurements were performed at D11, ILL.

Figure 2a displays the SAXS spectra obtained for R = 0.5 and R = 0.25, i.e. with 2 and 4 AuNP per liposome on average. For both samples the scattering due to liposomes is not distinguishable from the water background at these concentrations (green curve), and the signal is exclusively due to AuNP, either single or aggregated. When liposomes are present, the scattered intensity shows a clear q^{-2} trend in the low-q range, (Figure 2a, inset), superimposed to the form factor of primary AuNP, measured as a control sample. A quantitative estimation of the low-q slope, obtained by fitting the experimental AuNP-liposomes curves in Figure 2 to a multiple level Guinier-Porod model[30], can be found at Page S14 of SI. The occurrence of this power-law behavior hints at a fractal arrangement of the primary particles[31], not observed in the absence of liposomes.

The R = 0.25 sample was also imaged through AFM in liquid[32]. Figure 2b shows an example of extended assembly of AuNP on lipid vesicles (or vesicle aggregates), which corroborates the SAXS analysis. AFM does not allow determining whether the aggregates are 3D clusters of AuNP or 2D membrane-supported clusters. In agreement with the literature,[33–35] we would expect a 3D compact arrangement of primary NP to give rise to a SAXS power law characterized by a decay exponent higher than 2. Therefore, the combination of AFM and SAXS results would be consistent with the formation of extended 2D clusters of AuNP tightly packed on the liposomes surface.

Since in these dispersions AuNP and liposomes have comparable concentrations, the formation of membrane-confined extended aggregates of AuNP on a single liposome implies a strongly uneven distribution of AuNP: some liposomes will be extensively coated by AuNP, while others will be devoid of particles.

This conclusion is supported at the ensemble level by SANS, performed on the same AuNP-POPC liposome complexes (Figure 2c). No significant variations are observed in the scattering profiles upon interaction with AuNP, in line with the hypothesis that the vast majority of the liposomes remain "undressed". On the other hand, AFM provides proof of consistent aggregation at the level of single complexes (Figure 2b).

This phenomenon, i.e., a spontaneous aggregation of AuNP only on a limited number of liposomes, is a key feature of membrane-templated aggregation of AuNP, whose peculiar aspects will be addressed in the next paragraph.

3.3. Distribution of AuNP among liposomes

We evaluated the distribution of AuNP among liposomes by determining the relative abundancy of single and aggregated AuNP from the UV-Vis spectra (Figure 1); the analysis was performed considering the spectral profiles as the convolution of the original plasmon resonance peak (centered at 521 nm) and an additional red-shifted peak due to aggregated AuNP (see page S19 of Supplementary Data Analysis for details).[36] The relative area of each peak can be considered as a rough estimate of the percentage of single and aggregated AuNP. Interestingly, even for $R > 1$, with liposomes in excess with respect to AuNP, this evaluation yields a high percentage of

aggregated AuNP: as an example, for R = 2, with a number density of liposomes double with respect to AuNP (see Figure 1), we found a percentage of aggregated AuNP of 44%. (see pages S19-S22 of SI for details).

To frame this result from a statistical perspective, we tried to estimate the probability of finding multiple AuNP on the same liposome as a function of R. For simplicity, we considered AuNP and liposomes as dimensionless objects that undergo irreversible and complete association. This description, yet very simple, is of general applicability and allows making no assumption on the nature of the interaction forces at stake.

In this scenario, the distribution probability of AuNP per liposome (Pj, with j>0 number of NP on the same liposome) is described through a Poisson distribution, employed in the past to describe the distribution of molecular probes in micellar dispersions [37] (see pages S15-S19 of SI for details):

$$Pj = \frac{R^{(1-j)} \times e^{-(1/R)} \times j}{j!} \qquad (1)$$

where R is the liposomes/AuNP number ratio, as previously defined. As described in eq.1, Pj represents the probability to find an AuNP sharing the same liposomal surface with other j-1 gold nanoparticles. Therefore, for each R experimentally investigated there is a finite probability for multiple AuNP occupancy on the same vesicle, whose relative weight strongly depends on the stoichiometry: according to eq.1, the probability of finding two or more AuNP on the same liposome increases with decreasing R, in line with the UV-Vis results (Figure 1a-c). Therefore, the qualitative dependence of AuNP aggregation on R can be understood in terms of enhanced probability of multiple occupancy.

However, the Poisson model definitively fails when a quantitative analysis is attempted: specifically, the AuNPs' aggregation extent, evaluated with eq.1., is systematically underestimated for each *R* investigated.

For example, for $R = 2$ this model predicts that the majority of liposomes (about 60%) will be unoccupied and that AuNPs will distribute among the remaining 40% liposomes (See equation S1 and Figure S5 a) for details) either associating as a 1:1 or multiple:1 AuNPs/liposome complex.

More specifically, the majority of AuNP (61%) should associate with liposomes in a 1:1 fashion, while 30% should occur as "pairs", and only 9% will exhibit $j > 2$ (see equation 1 and Figure S5 b) for details).

This description is clearly not consistent with SAXS and UV-Vis results, which point at marked multiple occupancy. In addition, the Poisson-based model does not consider the finite sizes of liposomes and AuNP, which would further drastically reduce the expected percentage of aggregated AuNP (comprising of both dimers and oligomers) to 1.6% for $R = 2$ (see pages S15-S19 of SI for details).

To summarize the results so far, besides energetic contributions for adhesion and clustering, two distinctive features emerge: (i) the kinetic control of binding and aggregation, which results in irreversible clustering; (ii) the strongly uneven distribution of AuNP aggregates on selected liposomes.

In order to better disentangle these aspects, we address more in detail two "chemical" factors which might have a major impact and, specifically, the nature of the AuNP coating (3.4) and the viscoelastic properties of the lipid membrane (3.5).

3.4. Role of ligand on AuNP-liposomes interaction

The nature of surface ligands mediates the interaction between NP surface and lipid interfaces, both for synthetic and natural membranes. It is well-established that a positively charged coating agent will promote a dramatic interaction of NP with biological or biomimetic interfaces [15,38–40]; likewise, it is known that surface coatings with large steric hindrance (as PEG) will inhibit interactions with lipid membranes [15,41,42]. For small anionic ligands, the nano-bio interaction pathway strongly depends on the chemical nature of the ligand itself. For instance, the phenomenon here investigated has been observed specifically for the citrate-coated AuNP. This suggests a possibly overlooked role of the ligand in AuNP-membrane interactions, which should be related to specific molecular features of citrate that discriminate its behavior with respect to other small anionic ligands.

This capping agent is physisorbed on NP surface and can be easily displaced through "ligand-exchange" reactions. The behavior of citrate as an exchangeable capping agent is well-known: citrate is often used as intermediate ligand to functionalize NP [43,44], it is easily exchanged to thiolated ligands and, recently, it has been also shown that it can be displaced by other non-covalent capping agents [45], such, for instance, adenine [46].

To better address this point and its implications for the case under study, we compared the behavior of citrate-capped AuNP and AuNP capped with a thiolated ligand of similar size and charge as citrate but poorly exchangeable (3-mercaptopropionic acid, MPA).

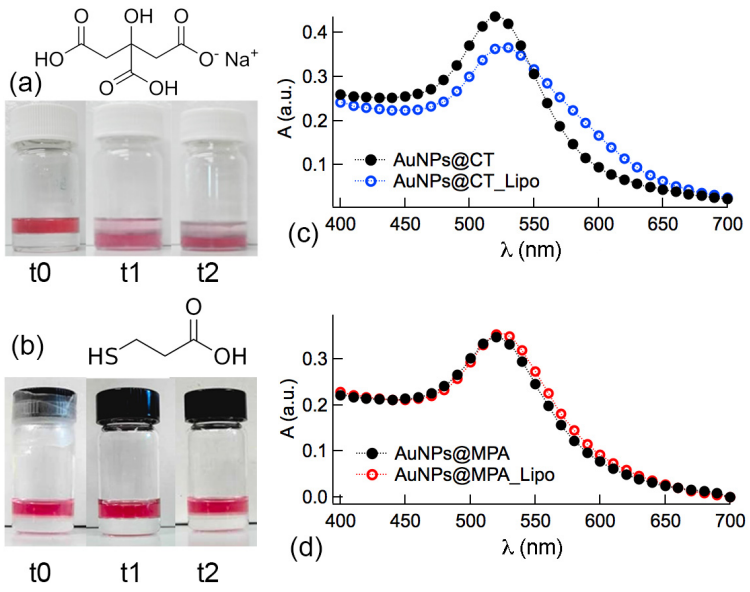

Figure 3. Role of citrate in the membrane-templated clustering of AuNP. (a, b) Photos of the two-phase system (NP + water)/(chloroform + POPC) of (a) AuNP@Ct and (b) AuNP@MPA captured: soon after chloroform addition (t0), after 20 min (t1) and 24 h (t2). (c, d) Representative UV-Vis spectra of R = 1 (c) AuNP@Ct and (d) AuNP@MPA before and after incubation with POPC liposomes.

To this purpose, we evaluated in a qualitative way the chemical affinity of citrated and MPA-coated AuNP towards POPC, i.e. the lipid component of vesicles, in a 1:1 (v:v) $CHCl_3$/water biphasic system. As a control experiment, we put in contact aqueous dispersions of MPA-capped AuNP or citrated AuNP with chloroform: even after 24 hours the organic phase is transparent, while the aqueous phase maintains its vivid color (see Figure S10 of SI for details). As expected, AuNP will be localized in water, due to their high surface charge density, imparted by the anionic ligands. If POPC is present in the organic phase (dissolved as a monomer at 1 mg/ml concentration), depending on the nature of ligands, we observe a dramatically different behavior.

While no significant variation is observed for MPA-AuNP with respect to the control experiment (Figure 3b), for citrate-capped AuNP the transfer of NP to the organic phase starts immediately and is complete after 24h (Figure 3a). The spectral properties of the organic phase indicate the presence of single primary AuNP (see Figure S9 of SI for details). The dispersion of NP in the organic phase is consistent with stabilization provided by a monolayer of POPC, with the hydrophilic zwitterionic headgroup on the particle surface and hydrophobic tails pointing towards the solvent.

This opposite behavior is clearly due to the fact that MPA is not exchanged with POPC, due to the strength of the Au-S bonds at the Au surface, while citrate is easily displaced by the lipid at the chloroform-water interface, where a monolayer of POPC is present, eventually leading to complete extraction of AuNP to the organic phase. This assay, even if qualitative, provides a clear and unambiguous indication that the affinity of AuNP for POPC strongly depends on the chemical nature of the ligand originally present on the NP.

Remarkably, this finding is strongly related to the behavior of AuNP when incubated with POPC liposomes in water: Figure 3c and 3d show the UV-Vis spectra of AuNP (citrate-capped, 3c and MPA-capped, 3d) added to liposome dispersions at R = 1. While the citrated AuNP exhibit the already discussed spectral redshift, the MPA-capped NP display a negligible variation of the absorption profile, which might be related to the adsorption of the NP on liposomal membrane [12], but definitely not to aggregation, occurring for citrated AuNP.

We put forward the hypothesis that also in this case the citrate-POPC exchange is a major player in the interaction between NP and POPC liposomes and subsequent NP clustering. The ligand

exchange at AuNP-liposome interface, with partial substitution of the citrate shell with POPC and release of citrate and counterions in water, would represent an irreversible binding step.

Therefore, the irreversible and kinetic nature of the lipid membrane binding and induced clustering, which is an unexplored key aspect in the liposomes/AuNP interaction, might find an explanation at a molecular level in the irreversible nature of citrate-POPC ligand exchange at the nano-bio interface.

3.5. Role of membrane elasticity on AuNP-liposomes interaction

Besides surface charge and composition [47,48], the phase state of the bilayer (gel or liquid crystalline) strongly affects the viscoelastic properties of the membrane and its response to NP adhesion. Recent studies addressed the interaction of citrated AuNP with lipid vesicles of similar composition as the system here considered (i.e., phosphatidylcholine phospholipids): the interaction of AuNP with lipid vesicles in gel and liquid crystalline phases was compared, either employing DPPC vesicles below and above the lipid membrane melting temperature (i.e., the gel to liquid crystalline transition temperature)[10], or considering vesicles of different lipid compositions at the same temperature (i.e. DOPC liquid crystalline and DPPC gel phase vesicles)[14]. Depending on the phase state of the membrane, aggregation of citrated AuNP was either inhibited (gel phase) or promoted (liquid crystalline phase). The authors have interpreted this result as due to a hampered lateral diffusion of the adhered AuNP when the target membrane is in the gel phase, which eventually limits aggregation. Therefore, the membrane lateral fluidity is considered the crucial factor to promote clustering of AuNP. Membrane fluidity modifications (particularly the formation of unstable lateral phase boundaries on fluid membranes upon citrated

AuNP adhesion) are also considered as a main driving force to AuNP clustering in another recent study [14]. While membrane fluidity can definitely play a role, other membrane viscoelastic properties might have been overlooked. Specifically, membrane bending rigidity is increasingly recognized as a key-factor which affects the reactivity of synthetic and natural bilayers towards nanomaterials [49,50]. The ability of a membrane to elastically deform and wrap around a NP, maximizing the interfacial contact area, is closely related to the balance between NP-bilayer adhesion energy and membrane bending energy (*viz*. elastic energy[49]), representing the energy cost for the bilayer to modify its spontaneous zero curvature. This balance determines the extent of NP wrapping and NP-membrane contact area, controlling the strength of interactions at the nano-bio interface [15,49–51].

Bending rigidity undergoes a dramatic variation passing from gel to liquid crystalline bilayers (for instance the bending moduli of fluid POPC and gel DPPC are $\approx 0.9 \times 10^{-19}$J and $\approx 15.5 \times 10^{-19}$J at 25°C, respectively[52]), which might have a crucial role in the interaction with AuNP.

To address this point, we determined the impact of membrane bending on membrane-templated clustering by monitoring POPC-AuNP interaction in systems where NP wrapping is hampered, due to high bending costs. We monitored POPC-AuNP hybrids obtained upon incubation of AuNP with POPC supported lipid bilayers (SLBs), obtained through vesicle fusion on a silicon wafer. The close interaction with the support prevents membrane bending, and in turn hinders AuNP wrapping by the membrane. Conversely, the lateral fluidity of POPC SLBs is retained or scarcely modified [53], as they are in the same physical state (i.e. liquid crystalline (fluid) state) as POPC

vesicles.. To rule out NP clusters formation due to the possible presence of residual intact liposomes on the SLB, all the samples were extensively washed after incubation.

Figure 4a compares the XRR [23] profiles of POPC SLBs in the absence and in the presence of AuNP. AuNP cause only a slight shift in the XRR oscillations of the bilayer form factor to lower q values, consistent with the adhesion of few NP on the lipid membrane (see curve fitting results in Table S2 of SI and the resulting scattering length density (SLD) profile along the bilayer thickness, Figure 4a inset) [54]. This finding is confirmed in real space with AFM images, where AuNP are embedded in the membrane as single objects or dimers (Figure 4c); in addition, QCM-D data (Figure 4d) show that, after the formation of a stable POPC SLB (Figure 4d, (1)) [27], the AuNP injection (2) results in the stable adsorption of some NP on the target membrane, with an overall coverage of approximately 3.5% of the SLB surface (see pages S9 of SI for details).

From these results, we conclude that AuNP adhere to the target membrane, but membrane-templated clustering of AuNP is significantly or completely limited, which points out a key role of membrane rigidity. We can conclude that the extent of NP wrapping by the membrane is one of the main factors driving the clustering of AuNP coated with citrate.

In order to further corroborate this result, we investigated the effect of AuNP size in the interaction with POPC liposomes.

While the adhesion energy per unit membrane is, to a first approximation, not dependent on the curvature locally imposed by the NP to the wrapping membrane[55], the bending energy per unit surface area of the bilayer (g_{be})[55,56] depends on the inverse of the NP radius square, as follows:

$$g_{be} = \frac{2}{r^2} k_c \qquad [2]$$

with k_c the bending modulus of the bilayer and r the NP radius.

To investigate the effect of reducing NP size we challenged POPC liposomes with significantly smaller citrated AuNP (5 nm instead of 16 nm in diameter, see paragraph 2 and page S2 of SI for details). Small AuNP impose an extremely high local curvature to the lipid membrane, whose deformation involves a higher energetic penalty with respect to 16 nm AuNP. Sharing the same exchangeable ligand, i.e. citrate, as 16 nm AuNP, small AuNP show the same affinity for POPC as bigger ones, as demonstrated by a control experiment in the biphasic water/chloroform system (see Figure S11 of SI for details); thus, the only difference between the two cases is then bending cost for unit area, which should result in a consistently lower wrapping for small NP (see equation 2).

Figure 4b displays an UV-Vis experiment similar to the one in Figure 1a, apart from the particle size: the plasmon coupling is here absent even for $R = 0.1$, suggesting that membrane adsorption might even occur, but membrane-templated aggregation is prevented. To summarize, 5 nm NP, which are expected to be wrapped by the membrane to a lower extent (Eq. 2), do not cluster, which confirms a major role of membrane bending elasticity in the citrated AuNP/liposome interaction.

To better interpret these results, we should consider that the bending capacity of the membrane determines its ability to bend and wrap around the NP, as highlighted in several recent studies [49,50]. Therefore, the wrapping extent of the NP determines the contact area between a NP and the membrane, where the citrate-POPC ligand exchange can take place.

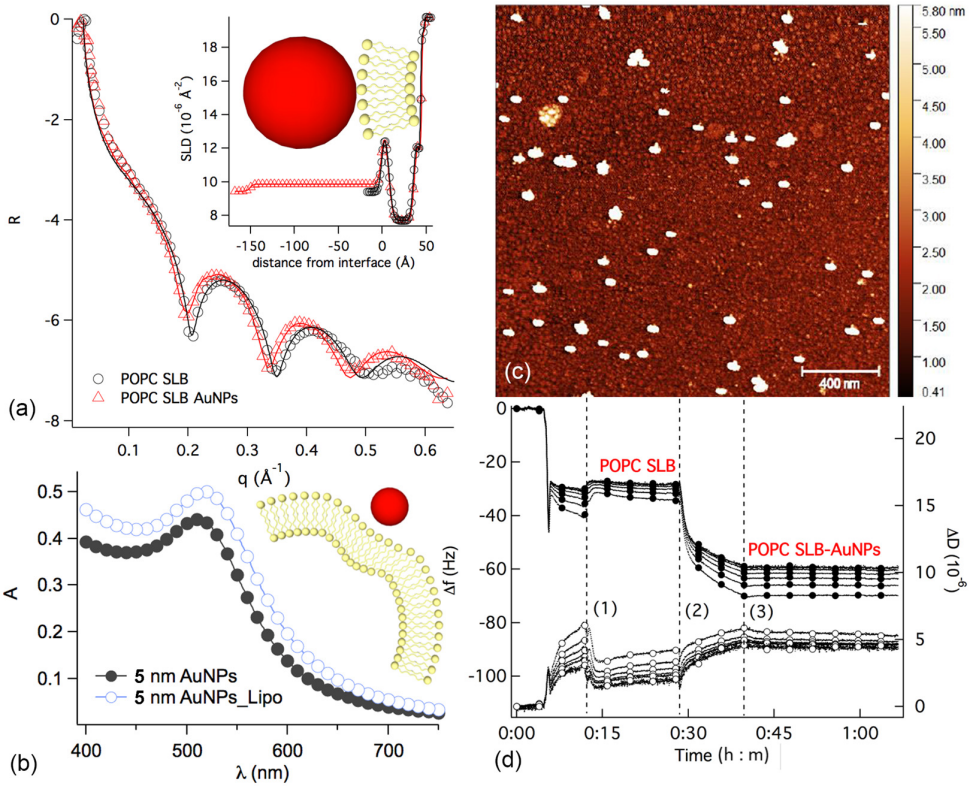

Figure 4. Wrapping contribution to membrane-templated AuNP clustering. (a) XRR profiles of a POPC SLB before and after incubation with AuNP; the curve fitting of the experimental curve and derived SLD profile (inset). (b) UV-vis plasmon resonance spectra of small-diameter (5 nm) citrated AuNP in the absence and in the presence of POPC liposomes for R = 0.1. (c) Liquid AFM of AuNP on a POPC SLB. (d) QCM-D experiment on the adsorption of AuNP on a POPC SLB: lines and filled circles represent the frequency shifts, while lines and empty circles represent the dissipation factors; the curves are normalized for the overtone numbers. XRR measurements were performed at ID03, ESRF.

Remarkably, increasing the contact area extension maximizes the portion of particle surface that will undergo citrate-POPC exchange. This ligand substitution will reduce the interparticle electrostatic repulsion on the membrane, enabling short-range NP-NP Van der Waals interactions, which can lead to the formation of 2D arrays of AuNP on the liposomal surface.

If wrapping is inhibited or limited by high bending costs, AuNP clustering is not observed, for the same coating and the same membrane: we attribute this effect to the lower POPC-citrate substitution on the NP surface, which prevents short-range interaction.

3.6. AuNP-liposomes interaction: a mechanistic hypothesis

The ensemble of experimental results reported here can be framed in a mechanistic hypothesis, which would account for the irreversible adsorption and 2D-clustering of AuNP on liposomes, and for the main driving energetic contributions.

(i) First adsorption of the AuNP drives bending of the lipid bilayer, which, by wrapping the AuNP, triggers irreversible POPC-citrate ligand exchange and in turn citrate and counterions' release in the NP immediate proximity.

(ii) the ligand exchange, decreasing NP-NP electrostatic repulsion, enables NP adhered to the same liposome to approach to distances at which Van der Waals attraction becomes effective, ultimately promoting AuNP ordered arrangement on the lipid membrane.

If this description explains the results presented here and those reported in the literature, one observation remains unclear, namely the strongly uneven distribution of AuNP among liposomes, which is not elucidated by statistical considerations (see paragraph 3.3) or by the mechanistic hypothesis above reported. Such an uneven distribution of AuNP membrane-confined clusters, present only on selected vesicles, implies the presence of a specific driving force, which acts cooperatively.

We put forward the hypothesis that a key contribution to this statistically unbalanced distribution is the release of citrate (and Stern counterions) at the liposome/NP interface, which follows POPC ligand exchange.

If the multivalent citrate ligands are released from the wrapped area of an AuNP (together with strongly-bound counterions), the ionic strength at the interface will locally and transiently increase to a significant extent. This local ionic strength increase will transiently decrease the Debye length, lowering the kinetic barrier for NP aggregation.

We can hypothesize that an iterative process takes place: the first AuNP binds randomly to the membrane, releasing a sufficient quantity of citrate anions to recruit another AuNP, which will adhere to the membrane and undergo the same extent of ligand exchange and citrate release, thereby trapping other AuNP. This will establish a preferential trail for AuNP towards a selected liposome and the distribution of NP will not be ruled by statistical considerations.

Unfortunately, to the best of our knowledge and expertise, it is not possible to perform an experiment which could directly probe a transient and localized increase of ionic strength in proximity of the adhesion point of a 16 nm AuNP on a single 100 nm liposome.

However, this iterative mechanism would be fully consistent with the experimentally observed connection between the extent of NP membrane wrapping and NP aggregation.

As a matter of fact, the increase of wrapping would also imply an increase of citrate release and, therefore, an increase in the efficiency of AuNP recruitment on a selected liposome.

This hypothesis scheme of a "citrate-trail" recruitment of AuNP would fit into a multistep model, such as the one sketched in Figure 5.

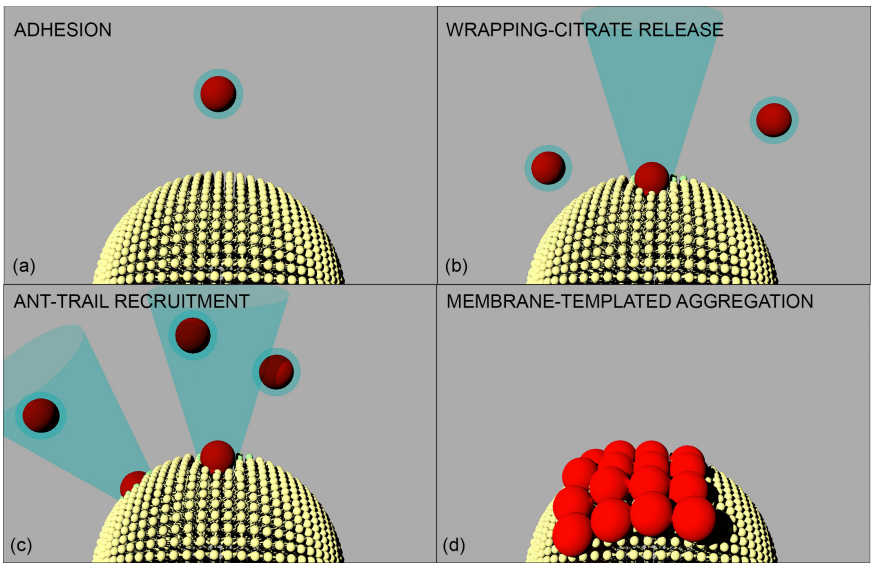

Figure 5. Mechanism of interaction between AuNP and the lipid membrane. (a) Adhesion-docking; (b) wrapping-ligand exchange; (c) citrate-trail recruitment; (d) Membrane-templated aggregation.

Within the DLVO formalism, accounting for both a long-range repulsive electrostatic potential and a short-range attractive London-Van der Waals potential, we outline the following interaction steps:

(i) Adhesion (i.e., AuNP docking to the liposomal membrane). The negative charge of AuNP, imparted by the citrate coating, provides a strong electrostatic repulsive contribution preventing short-range Van der Waals NP-NP interactions, while the electrostatic barrier for the adhesion of AuNP to the bilayer is significantly lower (POPC is zwitterionic, and liposomes have a slightly negative zeta potential). Thermal fluctuations can easily bring AuNP close to the bilayer, and eventually, adhesion driven by short-range liposome-AuNP attraction occurs.

(ii) Wrapping. Due to docking, a locally high curvature is imposed in the membrane. Depending on the NP size and on the bending modulus of the membrane, the NP is partially wrapped by the liposomal membrane, and irreversible ligand exchange between citrate and POPC occurs (which contributes to the kinetic-irreversible nature of citrated AuNP-lipid vesicles interaction). The extent of citrate displacement depends on the area wrapped by the membrane and therefore on the balance between the NP-membrane adhesion energy and the energy penalty due to membrane bending.

(iii) Citrate-trail. Wrapping causes the release of citrate and associated counterions, which determine a transient localized increase in the ionic strength. This action in turn increases the probability of the adhesion of another AuNP to the same liposome followed by a synergistic cascade effect, where each adhered AuNP partially releases its citrate coating to mark the membrane-adhesion pathway for the following AuNP.

(iv) Membrane-templated aggregation Once a relatively high number of AuNP are present on the same liposome, the decreased AuNP-AuNP electrostatic repulsion due to partial citrate release, together with the tendency of the membrane to decrease the locally imposed curvature due to AuNP adhesion, leads the formation of a curved membrane-confined AuNP aggregate on the lipid membrane.

4. CONCLUSIONS

We addressed the mechanistic features of the aggregation of citrate-coated gold nanoparticles (AuNP) on synthetic lipid membranes. This phenomenon, although recently highlighted in some

studies on nano-bio interfaces [10,12,13,18] and even exploited for bioanalytical assays [17], has never been fully disentangled and explained. Combining optical spectroscopy (UV-vis absorbance), bulk structural techniques (Small Angle Neutron and X-ray Scattering) and surface analysis (X-ray Reflectivity, Atomic Force Microscopy), we identified the main factors involved in the interaction of AuNP with synthetic lipid vesicles and the subsequent aggregation of NP. This allowed proposing a mechanistic hypothesis which would also explain and reconcile the data reported in the recent literature [10,14]. We disclose how thermodynamic (i.e., electrostatic and Van der Waals interactions, lipid membrane viscoelastic properties) and kinetic effects (citrate-lipid exchange at the nano-bio interface) are intertwined. For the first time, we suggest the key role of citrate and citrate-lipid ligand exchange to drive aggregation. This mechanism would imply that a small coating molecule, i.e., citrate, drives the response of a target lipid membrane to NP adhesion, resembling, in a very simple system, the mechanisms of small-molecule-activated biological responses in cell signaling phenomena. Moreover, the cooperative nature of ligand exchange at the AuNP-liposome interface, pivotal in determining clustering of AuNP, will have relevant implications for NP use in Nanomedicine, since NPs will be internalized in cells as clusters, rather than as primary NP, with dramatic effects on their bioactivity.

ACKNOWLEDGEMENTS

Funding Sources: ECRF (Ente Cassa di Risparmio di Firenze) and evFOUNDRY (H2020-FETOPEN-2016-2017—Project ID: 801367). AFM experiments were performed at the SPM@ISMN microscopy facility in Bologna and at the Partnership for Soft Condensed Matter (PSCM), Grenoble with the help of Marie Capron and Alain Panzarella. The Partnership for Soft

Condensed Matter (PSCM) is also gratefully acknowledged for QCM-D and Dynamic Light Scattering measurements; CM acknowledges ECRF (Ente Cassa di Risparmio di Firenze) and evFOUNDRY (H2020-FETOPEN-2016-2017—Project ID: 801367) for a financial support. The following DOI: 10.5291/ILL-DATA.9-13-597 identifies SANS experimental data acquired at ILL. 2016-2017—Project ID: 801367) for a financial support. The following DOI: 10.5291/ILL-DATA.9-13-597 identifies SANS experimental data acquired at ILL.

ASSOCIATED CONTENT

Supplementary Information including: Supplementary Materials and Methods section, Supplementary characterization of liposomes and NP, Supplementary Data Analysis are available online at JCIS website.

REFERENCES

(1) Henriksen-Lacey, M.; Carregal-Romero, S.; Liz-Marzán, L. M. Current Challenges toward in Vitro Cellular Validation of Inorganic Nanoparticles. *Bioconjug. Chem.* **2017**, *28* (1), 212–221. https://doi.org/10.1021/acs.bioconjchem.6b00514.

(2) Nel, A. E.; Mädler, L.; Velegol, D.; Xia, T.; Hoek, E. M. V; Somasundaran, P.; Klaessig, F.; Castranova, V.; Thompson, M. Understanding Biophysicochemical Interactions at the Nano-Bio Interface. *Nat. Mater.* **2009**, *8* (7), 543–557. https://doi.org/10.1038/nmat2442.

(3) Fox, L. J.; Richardson, R. M.; Briscoe, W. H. Historical Perspective PAMAM Dendrimer - Cell Membrane Interactions. *Adv. Colloid Interface Sci.* **2018**, *257*, 1–18. https://doi.org/10.1016/j.cis.2018.06.005.

(4) Beddoes, C. M.; Case, C. P.; Briscoe, W. H. Understanding Nanoparticle Cellular Entry: A Physicochemical Perspective. *Adv. Colloid Interface Sci.* **2015**, *218*, 48–68. https://doi.org/10.1016/j.cis.2015.01.007.

(5) Rossi, G.; Barnoud, J.; Monticelli, L. Polystyrene Nanoparticles Perturb Lipid Membranes.

J. Phys. Chem. Lett. **2014**, *5* (1), 241–246. https://doi.org/10.1021/jz402234c.

(6) Simonelli, F.; Bochicchio, D.; Ferrando, R.; Rossi, G. Monolayer-Protected Anionic Au Nanoparticles Walk into Lipid Membranes Step by Step. *J. Phys. Chem. Lett.* **2015**, *6* (16), 3175–3179. https://doi.org/10.1021/acs.jpclett.5b01469.

(7) Su, C. F.; Merlitz, H.; Rabbel, H.; Sommer, J. U. Nanoparticles of Various Degrees of Hydrophobicity Interacting with Lipid Membranes. *J. Phys. Chem. Lett.* **2017**, *8* (17), 4069–4076. https://doi.org/10.1021/acs.jpclett.7b01888.

(8) Gkeka, P.; Sarkisov, L.; Angelikopoulos, P. Homogeneous Hydrophobic-Hydrophilic Surface Patterns Enhance Permeation of Nanoparticles through Lipid Membranes. *J. Phys. Chem. Lett.* **2013**, *4* (11), 1907–1912. https://doi.org/10.1021/jz400679z.

(9) Mendozza, M.; Caselli, L.; Berti, D.; Salvatore, A. Nanoparticles and Organized Lipid Assemblies : From Interaction to Design of Hybrid Soft Devices Inorganic Stimuli Responsive. *Soft Matter* **2019**, *15* (44), 8951–8970. https://doi.org/10.1039/c9sm01601e.

(10) Sugikawa, K.; Kadota, T.; Yasuhara, K.; Ikeda, A. Anisotropic Self-Assembly of Citrate-Coated Gold Nanoparticles on Fluidic Liposomes. *Angew. Chemie - Int. Ed.* **2016**, *55* (12), 4059–4063. https://doi.org/10.1002/anie.201511785.

(11) Liu, J. Interfacing Zwitterionic Liposomes with Inorganic Nanomaterials: Surface Forces, Membrane Integrity, and Applications. *Langmuir* **2016**, *32* (18), 4393–4404. https://doi.org/10.1021/acs.langmuir.6b00493.

(12) Wang, F.; Liu, J. Self-Healable and Reversible Liposome Leakage by Citrate-Capped Gold Nanoparticles: Probing the Initial Adsorption/Desorption Induced Lipid Phase Transition. *Nanoscale* **2015**, *7* (38), 15599–15604. https://doi.org/10.1039/C5NR04805B.

(13) Montis, C.; Maiolo, D.; Alessandri, I.; Bergese, P.; Berti, D. Interaction of Nanoparticles with Lipid Membranes: A Multiscale Perspective. *Nanoscale* **2014**, *6* (12), 6452–6457. https://doi.org/10.1039/C4NR00838C.

(14) Wang, F.; Curry, D. E.; Liu, J. Driving Adsorbed Gold Nanoparticle Assembly by Merging Lipid Gel/Fluid Interfaces. *Langmuir* **2015**, *31* (49), 13271–13274. https://doi.org/10.1021/acs.langmuir.5b03606.

(15) Montis, C.; Generini, V.; Boccalini, G.; Bergese, P.; Bani, D.; Berti, D. Model Lipid Bilayers Mimic Non-Specific Interactions of Gold Nanoparticles with Macrophage Plasma Membranes. *J. Colloid Interface Sci.* **2018**, *516*, 284–294. https://doi.org/10.1016/j.jcis.2018.01.064.

(16) Canton, I.; Battaglia, G. Endocytosis at the Nanoscale. *Chem. Soc. Rev.* **2012**, *41* (7), 2718. https://doi.org/10.1039/c2cs15309b.

(17) Maiolo, D.; Paolini, L.; Di Noto, G.; Zendrini, A.; Berti, D.; Bergese, P.; Ricotta, D. Colorimetric Nanoplasmonic Assay to Determine Purity and Titrate Extracellular Vesicles.

Anal. Chem. **2015**, *87* (8), 4168–4176. https://doi.org/10.1021/ac504861d.

(18) Sugikawa, K.; Kadota, T.; Matsuo, K.; Yasuhara, K.; Ikeda, A. Growth of Anisotropic Gold Nanoparticle Assemblies via Liposome Fusion. *Materials (Basel).* **2017**, *10* (11), 1–10. https://doi.org/10.3390/ma10111317.

(19) Turkevich, J.; Stevenson, P. C.; Hillier, J. A Study of the Nucleation and Growth Processes in the Synthesis of Colloidal Gold. *Discuss. Faraday Soc.* **1951**, *11* (0), 55–75. https://doi.org/10.1039/DF9511100055.

(20) Frens, G. Controlled Nucleation for the Regulation of the Particle Size in Monodisperse Gold Suspensions. *Nat. Phys. Sci.* **1973**, *241*, 20–22. https://doi.org/10.1038/physci241020a0.

(21) Piella, J.; Bastús, N. G.; Puntes, V. Size-Controlled Synthesis of Sub-10-Nanometer Citrate-Stabilized Gold Nanoparticles and Related Optical Properties. *Chem. Mater.* **2016**, *28* (4), 1066–1075. https://doi.org/10.1021/acs.chemmater.5b04406.

(22) Kline, S. R. Reduction and Analysis of SANS and USANS Data Using IGOR Pro. *J. Appl. Crystallogr.* **2006**, *39* (6), 895–900. https://doi.org/10.1107/S0021889806035059.

(23) Gumí-Audenis, B.; Costa, L.; Redondo-Morata, L.; Milhiet, P. E.; Sanz, F.; Felici, R.; Giannotti, M. I.; Carlà, F. In-Plane Molecular Organization of Hydrated Single Lipid Bilayers: DPPC: Cholesterol. *Nanoscale* **2018**, *10* (1), 87–92. https://doi.org/10.1039/c7nr07510c.

(24) Gumí-Audenis, B.; Carlà, F.; Vitorino, M. V.; Panzarella, A.; Porcar, L.; Boilot, M.; Guerber, S.; Bernard, P.; Rodrigues, M. S.; Sanz, F.; et al. Custom AFM for X-Ray Beamlines: In Situ Biological Investigations under Physiological Conditions. *J. Synchrotron Radiat.* **2015**, *22* (6), 1364–1371. https://doi.org/10.1107/S1600577515016318.

(25) Ainalem, M. L.; Campbell, R. A.; Nylander, T. Interactions between DNA and Poly(Amido Amine) Dendrimers on Silica Surfaces. *Langmuir* **2010**, *26*, 8625–8635. https://doi.org/10.1021/la9047177.

(26) Rodahl, M.; Höök, F.; Fredriksson, C.; Keller, C. A.; Krozer, A.; Brzezinski, P.; Voinova, M.; Kasemo, B. Simultaneous Frequency and Dissipation Factor QCM Measurements of Biomolecular Adsorption and Cell Adhesion. *Faraday Discuss.* **1997**, *107*, 229–246. https://doi.org/10.1039/a703137h.

(27) Montis, C.; Gerelli, Y.; Fragneto, G.; Nylander, T.; Baglioni, P.; Berti, D. Nucleolipid Bilayers: A Quartz Crystal Microbalance and Neutron Reflectometry Study. *Colloids Surfaces B Biointerfaces* **2016**, *137*, 203–213. https://doi.org/10.1016/j.colsurfb.2015.07.039.

(28) Wang, B.; Zhang, L.; Chul, S.; Granick, S. Nanoparticle-Induced Surface Reconstruction of Phospholipid Membranes. *Natl. Acad. Sci. United States Am.* **2008**, *105* (47), 18171–

18175. https://doi.org/https://doi.org/10.1073/pnas.0807296105.

(29) Pfeiffer, T.; De Nicola, A.; Montis, C.; Carlà, F.; van der Vegt, N. F. A.; Berti, D.; Milano, G. Nanoparticles at Biomimetic Interfaces: Combined Experimental and Simulation Study on Charged Gold Nanoparticles/Lipid Bilayer Interfaces. *J. Phys. Chem. Lett.* **2018**, 129–137. https://doi.org/10.1021/acs.jpclett.8b03399.

(30) Hammouda, B. A New Guinier – Porod Model. *J. Appl. Crystallogr.* **2010**, *43* (4), 716–719. https://doi.org/10.1107/S0021889810015773.

(31) Feigin, L. A.; Svergun, D. S. *Structure Anaysis by Small Angle X-Ray and Neutron Scattering*; Taylor, G. W., Ed.; Plenum Press, New York: Princeton, 1987.

(32) Antosova, A.; Gazova, Z.; Fedunova, D.; Valusova, E.; Bystrenova, E.; Valle, F.; Daxnerova, Z.; Biscarini, F.; Antalik, M. Anti-Amyloidogenic Activity of Glutathione-Covered Gold Nanoparticles. *Mater. Sci. Eng. C* **2012**, *32* (8), 2529–2535. https://doi.org/10.1016/j.msec.2012.07.036.

(33) Lazzari, S.; Nicoud, L.; Jaquet, B.; Lattuada, M.; Morbidelli, M. Fractal-like Structures in Colloid Science. *Adv. Colloid Interface Sci.* **2016**, *235*, 1–13. https://doi.org/10.1016/j.cis.2016.05.002.

(34) Sui, J.; Zhao, P.; Bin-Mohsin, B.; Zheng, L.; Zhang, X.; Cheng, Z.; Chen, Y.; Chen, G. Fractal Aggregation Kinetics Contributions to Thermal Conductivity of Nano-Suspensions in Unsteady Thermal Convection. *Sci. Rep.* **2016**, *6*, 39446. https://doi.org/10.1038/srep39446.

(35) Thouy, R.; Jullien, R. Structure Factors for Fractal Aggregates Built Off-Lattice with Tunable Fractal Dimension. *J. Phys. I* **2003**, *6* (10), 1365–1376. https://doi.org/10.1051/jp1:1996141.

(36) Sharma, V.; Chotia, C.; Tarachand; Ganesan, V.; Okram, G. S. Influence of Particle Size and Dielectric Environment on the Dispersion Behaviour and Surface Plasmon in Nickel Nanoparticles. *Phys. Chem. Chem. Phys.* **2017**. https://doi.org/10.1039/c7cp01769c.

(37) Hunter, R. J. Foundations of Colloid Science. *Oxford Univ. Press Inc., New York,* **2001**, Page 472 (Exercise 9.6.1.). https://doi.org/10.1016/S0927-7757(02)00170-X.

(38) Tatur, S.; Maccarini, M.; Barker, R.; Nelson, A.; Fragneto, G.; Wang, B.; Zhang, L.; Bae, S. C.; Granick, S.; Yu, Y.; et al. Effect of Functionalized Gold Nanoparticles on Floating Lipid Bilayers. *Environ. Sci. Technol.* **2008**, *48* (2), 873–880. https://doi.org/10.1021/es403864v.

(39) Lolicato, F.; Joly, L.; Martinez-Seara, H.; Fragneto, G.; Scoppola, E.; Baldelli Bombelli, F.; Vattulainen, I.; Akola, J.; Maccarini, M. The Role of Temperature and Lipid Charge on Intake/Uptake of Cationic Gold Nanoparticles into Lipid Bilayers. *Small* **2019**, *15* (23), 1805046. https://doi.org/10.1002/smll.201805046.

(40) Pfeiffer, T.; De Nicola, A.; Montis, C.; Carlà, F.; Van Der Vegt, N. F. A.; Berti, D.; Milano, G. Nanoparticles at Biomimetic Interfaces: Combined Experimental and Simulation Study on Charged Gold Nanoparticles/Lipid Bilayer Interfaces. *J. Phys. Chem. Lett.* **2019**, *10* (2), 129–137. https://doi.org/10.1021/acs.jpclett.8b03399.

(41) Park, Y. C.; Smith, J. B.; Pham, T.; Whitaker, R. D.; Sucato, C. A.; Hamilton, J. A.; Bartolak-Suki, E.; Wong, J. Y. Effect of PEG Molecular Weight on Stability, T2 Contrast, Cytotoxicity, and Cellular Uptake of Superparamagnetic Iron Oxide Nanoparticles (SPIONs). *Colloids Surfaces B Biointerfaces* **2014**, *119*, 106–114. https://doi.org/10.1016/j.colsurfb.2014.04.027.

(42) García, K. P.; Zarschler, K.; Barbaro, L.; Barreto, J. A.; O'Malley, W.; Spiccia, L.; Stephan, H.; Graham, B. Zwitterionic-Coated "Stealth" Nanoparticles for Biomedical Applications: Recent Advances in Countering Biomolecular Corona Formation and Uptake by the Mononuclear Phagocyte System. *Small* **2014**, *10* (13), 2516–2529. https://doi.org/10.1002/smll.201303540.

(43) Zhu, T.; Vasilev, K.; Kreiter, M.; Mittler, S.; Knoll, W. Surface Modification of Citrate-Reduced Colloidal Gold Nanoparticles with 2-Mercaptosuccinic Acid. *Langmuir* **2003**, *19*, 9518–9525. https://doi.org/10.1021/la035157u.

(44) Rana, K.; Bhamore, J. R.; Rohit, J. V.; Park, T. J.; Kailasa, S. K. Ligand Exchange Reactions on Citrate-Gold Nanoparticles for a Parallel Colorimetric Assay of Six Pesticides. *New J. Chem.* **2018**, *42*, 9080–9090. https://doi.org/10.1039/c8nj01294f.

(45) Wang, X.; Wang, X.; Bai, X.; Yan, L.; Liu, T.; Wang, M.; Song, Y.; Hu, G.; Gu, Z.; Miao, Q.; et al. Nanoparticle Ligand Exchange and Its Effects at the Nanoparticle-Cell Membrane Interface. *Nano Lett.* **2019**, *19* (1), 8–18. https://doi.org/10.1021/acs.nanolett.8b02638.

(46) Perera, G. S.; Athukorale, S. A.; Perez, F.; Pittman, C. U.; Zhang, D. Facile Displacement of Citrate Residues from Gold Nanoparticle Surfaces. *J. Colloid Interface Sci.* **2018**, *511*, 335–343. https://doi.org/10.1016/j.jcis.2017.10.014.

(47) Lunnoo, T.; Assawakhajornsak, J.; Puangmali, T. In Silico Study of Gold Nanoparticle Uptake into a Mammalian Cell: Interplay of Size, Shape, Surface Charge, and Aggregation. *J. Phys. Chem. C* **2019**, *123* (6), 3801–3810. https://doi.org/10.1021/acs.jpcc.8b07616.

(48) Ingo, H. I.; Melo, M. N.; Eerden, F. J. Van; Lopez, C. A.; Wassenaar, T. A.; Periole, X.; Vries, A. H. De; Tieleman, D. P.; Marrink, S. J. Lipid Organization of the Plasma Membrane. *J. Am. Chem. Soc.* **2014**, *136* (41), 14554–14559.

(49) Bahrami, A. H.; Raatz, M.; Agudo-Canalejo, J.; Michel, R.; Curtis, E. M.; Hall, C. K.; Gradzielski, M.; Lipowsky, R.; Weikl, T. R. Wrapping of Nanoparticles by Membranes. *Adv. Colloid Interface Sci.* **2014**, *208*, 214–224. https://doi.org/10.1016/j.cis.2014.02.012.

(50) Michel, R.; Gradzielski, M. Experimental Aspects of Colloidal Interactions in Mixed Systems of Liposome and Inorganic Nanoparticle and Their Applications. *Int. J. Mol. Sci.* **2012**, *13* (9), 11610–11642. https://doi.org/10.3390/ijms130911610.

(51) Agudo-Canalejo, J.; Lipowsky, R. Critical Particle Sizes for the Engulfment of Nanoparticles by Membranes and Vesicles with Bilayer Asymmetry. *ACS Nano* **2015**, *9* (4), 3704–3720. https://doi.org/10.1021/acsnano.5b01285.

(52) Et-Thakafy, O.; Delorme, N.; Gaillard, C.; Mériadec, C.; Artzner, F.; Lopez, C.; Guyomarch, F. Mechanical Properties of Membranes Composed of Gel-Phase or Fluid-Phase Phospholipids Probed on Liposomes by Atomic Force Spectroscopy. *Langmuir* **2017**, *33* (21), 5117–5126. https://doi.org/10.1021/acs.langmuir.7b00363.

(53) Guo, L.; Har, J. Y.; Sankaran, J.; Hong, Y.; Kannan, B.; Wohland, T. Molecular Diffusion Measurement in Lipid Bilayers over Wide Concentration Ranges: A Comparative Study. *ChemPhysChem* **2008**, *9* (5), 721–728. https://doi.org/10.1002/cphc.200700611.

(54) Nelson, A. Co-Refinement of Multiple-Contrast Neutron/X-Ray Reflectivity Data Using MOTOFIT. *J. Appl. Crystallogr.* **2006**, *39* (2), 273–276. https://doi.org/10.1107/S0021889806005073.

(55) Raatz, M.; Lipowsky, R.; Weikl, T. R. Cooperative Wrapping of Nanoparticles by Membrane Tubes. *Soft Matter* **2014**, *10* (20), 3570–3577. https://doi.org/10.1039/c3sm52498a.

(56) Sackmann, E. Membrane Bending Energy Concept of Vesicle- and Cell-Shapes and Shape-Transitions. *FEBS Lett.* **1994**, *346* (1), 3–16.